Removal of Methyl Orange from Aqueous Solution Using Zeolitic Imidazolate Framework-11: Adsorption Isotherms, Kinetics and Error Analysis

Lamari, Rachid*[+]***; Benotmane, Benamar***
URMPE, M'Hamed Bougara University, Boumerdes, 35000, ALGERIA

Mostefa, Farida
Faculty of sciences, Department of chemistry, M'Hamed Bougara University, Boumerdes, 35000, ALGERIA

ABSTRACT: *Dyes, which are increasingly harmful to human health and ecology, are an environmental concern and their removal from wastewater is extremely required. It is also important for researchers to find relevant techniques to process these types of pollutants. This study examines the use of the synthesized imidazolate zeolite frameworks-11 (ZIF-11) by stirring method for the Methyl Orange (MO) dye removal from an aqueous solution. Scanning electron microscopy, thermogravimetry, X-ray diffraction, and Fourier transform infrared spectroscopy, were used for the analysis of ZIF-11 particles, which exhibited highly porous, irregular, and heterogeneous shapes and variable sizes. The MO removal was assessed by batch adsorption with ZIF-11 particles as adsorbent, whose efficiency was achieved at pH=8, stirring speed of 600 rpm, for a contact time of 40min, and a dosage of 800mg/L of MO solution. The thermodynamic and kinetic analysis of the MO adsorption process was achieved successfully with the pseudo-second-order kinetic model as well as Langmuir and Temkin isotherms, indicating the feasibility and spontaneity of the uniform distribution of MO molecules on the active sites of ZIF-11 particles. The calculated maximum adsorption capacity of MO on ZIF-11 particles was 178.57 mg/g, which is indicative of the potential adsorptive properties of the synthesized ZIF-11 for MO dyes.*

KEYWORDS: *Methyl orange; ZIF-11; Isotherm; Kinetics; Thermodynamic; Error analysis.*

INTRODUCTION

Zeolitic Imidazolate Frameworks (ZIFs) represent a special class of Metal-Organic Frameworks (MOFs), formed by imidazolate linkers and zinc or cobalt ions, resulting in microporous crystalline structures with characteristics of both MOFs and zeolites [1,2]. ZIFs possess unique porous structures with open frameworks, adjustable cage pore structures, large surface areas, abundant functionalities, and enhanced thermal and chemical stabilities, which led them to a wide range of potential applications including adsorption, catalysis,

***** *To whom correspondence should be addressed.*
+ E-mail: r.lamari@univ-boumerdes.dz
1021-9986/2022/6/1985-1999 15/$/6.05

separation, and sensing [3-8]. In particular, ZIF-11 is consisting of Zn atoms coordinated with nitrogen atoms of benzimidazole (bIM) forming a crystalline and microporous structure with RHO-type topology and large pores 14.6 Å in diameter connected through small apertures of 3 Å across [1]. This important structural feature combined with the remarkable chemical and thermal stability of this component provides a variety and abundance of applications. Many works highlight the use of ZIF-11 and their derivatives in the adsorption of alcohol and hydrocarbon vapors [9], selective adsorption, and separation of inert gases (Xenon and Krypton) [10], in mixed-matrix membranes technology [11], or as a photocatalyst to decompose methylene blue under UV light irradiation [12]. Obviously, as ZIFs are high-performance adsorbents for various substances, they should be investigated for pollutants such as dyes.

Huge amounts of highly colored effluent are discharged into industrial wastewater, especially from the textile, printing, plastics, and dye synthesis industries. In view of their non-biodegradable, recalcitrant, and harmful nature, these pollutants remain the utmost environmental concern. Dyes removal from wastewater can be achieved by conventional physical methods such as adsorption, coagulation or flocculation, ion exchange, irradiation, membrane filtration, nanofiltration or ultra-filtration, and reverse osmosis [13]. The method of dye removal by adsorption is a highly efficient technique, which easily degrades almost all of the dyes or their mixtures when carried out with the use of appropriate adsorbents such as activated carbon [14], magnetic iron- manganese oxide coated graphene oxide [15], ZnO–Al_2O_3 nanocomposite [16], and ZIF-67 [17]. In this context, Methyl Orange (MO) dyes extensively employed in textile, paper, printing, leather, cosmetics, and food industries are mostly discharged in industrial wastewater [18]. MO is a benzenesulfonic acid anionic mono-azo dye, which may affect human health in many ways, such as carcinogenicity, genotoxicity, mutagenicity, increased heart rate, vomiting, and shock [19, 20]. Moreover, synthetic origin, aromatic ring structure, oxidation reaction, and azo link make the MO dye difficult to degrade [21, 22]. Some studies have been reported on the removal of MO from aqueous solutions [23-26]. The results showed that the adsorption occurred spontaneously and that under optimal conditions, the percentage of MO removal was 97% at an equilibrium time of 30 min.

However, to the best of our knowledge, the use of MOFs or ZIFs for the removal of dyes from wastewater well known for their environmentally negative incidence has been poorly investigated; in particular, ZIF-11 remains the least reported. Nevertheless, ZIF-8 and ZIF-67 have displayed good adsorption performance towards some dyes due to their positive Zeta potential at a wide pH range or some special functional groups like -SO_3 of dyes [4, 17, 26, 27]. In view of these findings, it will be appropriate to explore the performance of ZIF-11 as an adsorbent of MO dyes. Therefore, the main objective of this study is to evaluate a synthesized ZIF-11 for the MO dye adsorption from an aqueous solution.

EXPERIMENTAL SECTION

Instruments

During experiments, the MO concentration was evaluated at 464 nm (using UV-Visible spectrophotometer model PG INSTRUMENTS T60) based on a respective linear calibration curve over desired understudy concentration range. The pH of the sample solution was adjusted by the addition of HCl or NaOH using a pH meter model-8603 Seven Easy, METTLER TOLEDO, Switzerland.

Chemicals

Zinc acetate dihydrate ($Zn(CH_3)_2.2H_2O$, >99.99%, E.MERCK, Germany), Benzimidazole ($C_7H_6N_2$, 98%), and methanol (CH_3OH, 99.8%) were purchased from Sigma–Aldrich INDIA, ammonium hydroxide (NH_3, 25% aqueous solution) was purchased from BIOCHEM Chemopharma, toluene ($C_6H_5CH_3$, 98.8%, Panreac), methyl orange was bought from Chemical Reagent of the National Chinese Pharmaceutical Group Co., Ltd., deionized water with a conductivity of 6 $x10^{-2}$ µS/cm was used in the preparation of all samples and standards. All the chemicals were analytical-grade reagents and were used without further purification.

Preparation of the adsorbent

ZIF-11 crystal was synthesized at room temperature (20 ±2 °C), in a purely aqueous system by the procedure reported in the given references [28-30]. Benzimidazole (5.079 mmol) was dissolved in methanol (522.784 mmol) and ammonia (107.020 mmol), separately, zinc acetate dihydrate (2.506 mmol) was dissolved in methanol (524.344 mmol) and toluene (141.089 mmol).

The obtained solutions were mixed under stirring. This mixture was gently stirred (200 rpm) in a vial (100 mL) for two hours (02 h), to obtain a white precipitate: the ZIF-11, which was collected by centrifugation, washed with methanol, and dried in an oven at 120 °C overnight to evaporate the trapped toluene and methanol (yield: 0.1422 g, R>89.70%).

Preparation of Methyl orange solution

The MO stock solution (1000 mg/L) was prepared by dissolving a precisely weighed mass of MO in distilled water. By diluting the stock solution with distilled water all adsorption test solutions of the desired concentrations were made and the pH was adjusted by adding analytical concentration grade NaOH and HCl solutions (purchased from Sigma-Aldrich INDIA).

Point of zero charges (pHzpc) determination

Six separate 150 mL Erlenmeyer flasks were filled with a sodium chloride solution (50 mL, 0.01 M) and the initial pH (pH_i) was adjusted to between 2.0 and 12.0 by the addition of 0.1M HCl or NaOH. Subsequently, 0.15 g of ZIF-11 powder was introduced to each flask and placed under stirring for 24 h. The final pH (pH_f) of the samples was measured after centrifugation (400rpm). The (pH_i-pH_f) values were plotted against pH_i on a graph to determine the pH_{ZPC} at the crossover point of pH_i and (pH_i-pH_f).

Experimental procedure

The adsorption of MO on to ZIF-11 was performed in batch experiments. Adsorption experiments were performed in 100 mL (volume) of Erlenmeyer flasks containing 50 mL of MO solutions and the desired dose of ZIF-11 was charged and placed in a thermocouple incubator (IKA ® RCT basic safety control). To determine the efficiency of adsorption on ZIF-11, experiments were carried out while varying the adsorption parameters namely the solution pH, the contact time, the solution temperature, the amount of adsorbent, the initial concentration of dye, and the stirring speed. The following equation estimated the adsorptive capacity of the equilibrium:

$$q_e = \frac{(C_0 - C_e)}{W} \cdot V \qquad (1)$$

where:

q_e : is the adsorptive capacity at equilibrium, mg/g.

C_0: is the initial concentration of MO in the solution, mg./L.

C_e: is the concentration of MO in the solution at equilibrium, mg/L.

V: is the volume of the solution, L.

W: is the mass of the adsorbent (ZIF-11), g.

The MO removal percentage can be calculated according to the equation:

$$R(\%)_t = \left[\frac{(C_0 - C_t)}{C_0}\right] \cdot 100 \qquad (2)$$

Validity of adsorption isotherm and kinetic model

Adsorption modeling consists of determining the best fit that quantifies the distribution of adsorbates and verifying the consistency of adsorption models and their theoretical assumptions. In order to meet this objective, linear and non-linear regression analysis are the tools most frequently used for the statistical processing of experimental data [31, 32]. Linear regression analysis is carried out using the coefficient of determination. Non-linear regression analysis generally involves minimizing the distribution of errors between the experimental data and the isotherm predicted based on its convergence criteria. This operation requires easy-to-use computer algorithms such as the solver add-in program of Microsoft Excel. In this respect, the error functions and statistics involved are described below.

The coefficient of determination R^2 is used to analyze the fitting degrees of the linearized kinetic and isotherm models with experimental data. It is defined by the following equation:

$$R^2 = 1 - \frac{\sum_{i=1}^{N}\left[\left(q_{e,exp} - q_{e,cal}\right)^2\right]_i}{\sum_{i=1}^{N}\left[\left(q_{e,exp} - \overline{q_{e,exp}}\right)^2\right]_i} \qquad (3)$$

The Sum of Error Squares (SSE) is used in the least squares technique for the estimation of regression coefficients. It is a measure of the deviation between the experimental and the calculated data. It's given by the following equation :

$$SSE = \sum_{i=1}^{N}\left(q_{xp} - q_{cal}\right)^2 \qquad (4)$$

The Root Mean Square Error (RMSE) is a standard for measuring the deviation of predictive models from experimental data. A smaller RMSE value indicates that the model is well-fitted to the data. It is evaluated by the following equation:

$$\mathrm{RMSE} = \sqrt{\frac{1}{N}\sum_{i=1}^{N}\left(q_{exp} - q_{cal}\right)^2} \quad (5)$$

The Chi-square test ~~was~~ is used as a criterion for the quality of the fit of data to a model. The chi-square statistic (χ^2) is given by:

$$\chi^2 = \sum_{i=1}^{N}\frac{\left(q_{exp} - q_{cal}\right)^2}{q_{exp}} \quad (6)$$

The average relative error (ARE) is an error function, with the aim to decrease the fractional error distribution across the overall concentration range. It is determined by the equation

$$\mathrm{ARE} = \frac{100}{n}\sum_{i=1}^{N}\left|\frac{q_{exp} - q_{cal}}{q_{exp}}\right| \quad (7)$$

Marquardt's Percent Standard Deviation (MPSD) error function is similar to the geometric mean error distribution with $(N - P)$ degrees of freedom. It is defined by the equation

$$\mathrm{MPSD} = 100\sqrt{\frac{1}{N-P}\sum_{i=1}^{N}\left(\frac{q_{exp} - q_{cal}}{q_{exp}}\right)^2} \quad (8)$$

In these equations, q_{exp} (mg/g) is the experimental value of uptake, q_{cal} (mg/g) is the calculated value of uptake obtained from the model and N is the number of experimental data and P is the number of parameters in the regression model.

RESULTS AND DISCUSSION

Characterization of ZIF-11 synthesized

X-ray diffraction (XRD)

The crystallographic structure of ZIF-11 synthesized was analyzed using a PANalytical X-Pert Pro, Empyrean Cu LFF HR (9430 033 7310x) DK417340 with CuKa radiation at a scan rate of 2 °/min with a step size of 0.00 from 4.99 to 90 and λ = 1.54 Å. The accelerating voltage and applied currents were 45 kV and 40 mA, respectively.

The powder X-ray diffraction patterns of the synthesized ZIF-11 before adsorption (A), and after MO adsorption at 25°C (B) are shown in Fig.1 respectively. The synthesized samples showed a slight peak shift towards high angles of two thetas at 20° = 6.21° and 7.62° corresponding to planes (200) and (211) respectively. The structure of ZIF-11 being flexible, a decrease in interplanar spacing might occur as observed in several microporous crystals, including zeolitic imidazolate frameworks [17, 33]. The increased intensity of the main peaks corresponding to the (200) and (211) planes showed a higher crystallinity. However, no peak shift was observed in the XRD result of the samples after adsorption showing a stable structure. The characteristic peaks of ZIF-11 patterns matched well with those mentioned in the literature, indicating a highly crystalline structure [34-36].

Scanning electron microscope and energy-dispersive X-ray spectroscopy (SEM/EDAX) analysis of ZIF-11.

The prepared ZIF-11 microstructure was observed using scanning electron microscopy SEM (QUANTA 650). The material was deposited on an adhesive and conductive observation medium and then was metalized with argon plasma. The observation was carried out under a vacuum at an accelerating voltage of 05 kV. The surface morphology of ZIF-11 particles as shown in Fig.2 exhibited a highly porous, irregular, and heterogeneous shape and variable size.

The EDAX spectrum and elemental distribution with the atomic and weight percentage fraction for the synthesized ZIF-11 are presented in Fig. 3 and Table 1 respectively. The distinctive peaks in the spectrum include the atoms C, N, and Zn. The elemental analysis obtained from EDAX is close to the synthesis initial composition (expected theoretical values). The weak peak for O atom probably originated from the zinc acetate dihydrate and methanol used in the ZIF-11 synthesis. However, there are some discrepancies between the values given by the EDAX analysis for the synthesized ZIF-11 and the values obtained by other authors [12]; the surface imperfect crystallinity of the particles may influence the EDAX analysis results.

ThermoGravimetric Analysis and Differential Scanning Calorimetry (TGA/DSC)

To assess the physical and chemical stability of ZIF-11 particles, the thermal analysis was carried out in an N_2 atmosphere at a scan rate of 10 K/min from 50°C to 700°C

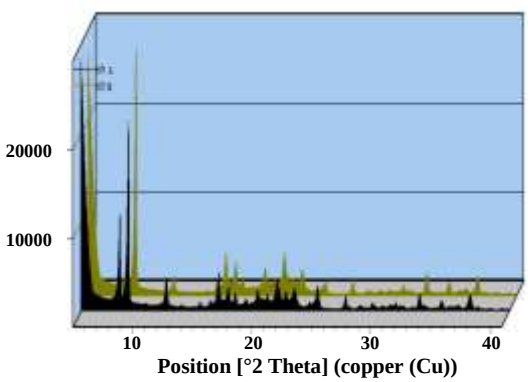

Fig. 1: 3D X-Ray patterns of ZIF-11 (A, before adsorption tests and B, after adsorption tests,) obtained after several times at 25°C.

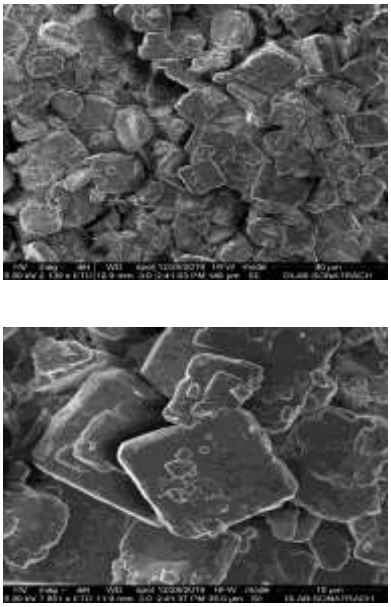

Fig. 2: Scanning electron microscope pictures of ZIF-11 particles : magnitude 2139 x (left) and 7851 x (right)

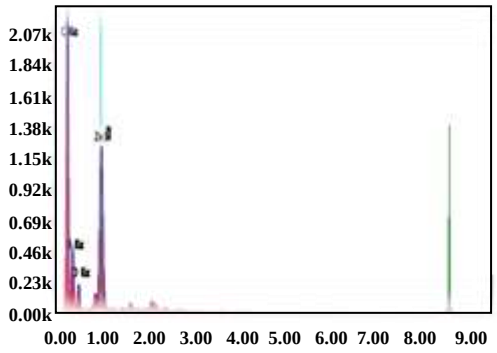

Fig.3: EDAX spectrum and elemental distribution of the synthesized ZIF-11.

on a NETZSCH STA 409PC/P. The obtained thermogravimetric analysis (TGA) and the Differential scanning calorimetry (DSC) diagrams showed that ZIF-11 particles were thermally stable up to 480 °C (Fig. 4). The skeleton of ZIF-11 exhibited high thermal stability. Then, a weight loss (8% by weight) was observed from 480°C to 540°C, due to the escape of guest molecules such as methanol as well as gas molecules from the cavities. A complete weight loss (71% by weight) occurred in the range of 540-645°C thereafter the mass of the sample remained almost constant suggesting the decomposition of ZIF-11 into zinc oxide (28 % by weight). Two exothermic peaks at 557°C and 643°C on the DSC curve supported this assumption; they corresponded to two-stage zinc oxidation in relation to irregular and variable crystal size. These results are in agreement with those observed in the literature [1, 28, 30, 37].

Fourier Transform InfraRed (FT-IR) spectroscopy

FT-IR spectroscopy was used to identify the main functional groups of the ZIF-11 synthesized samples. As shown in Figure 5, all frequencies related to the bonds within the bIM ring were available. The ZIF-11 crystals exhibited distinctive absorption bands at 3088, 3057, 3032 cm^{-1} (=C–H stretching of aromatics), and, 1465 cm^{-1} (C–C stretching in the aromatic ring). More intense peaks at 1606 cm^{-1} and 1547 cm^{-1} were attributed to C=C stretching. The bands occurring at around 530–400 cm^{-1} were fingerprints of ZnO. In particular, the band at 427 cm^{-1} corresponded to Zn–N stretching, and the peaks between 600 and 1500 cm−1 are related to the entire benzimidazole ring stretching or bending. Along these lines, these results proved the successful reaction of Zn^{+2} and bIM in ZIF-11 crystals [1, 28, 38, 39]. The occurrence in the bIM rings of both benzyl rings as electron acceptors and imidazole groups as electron donors will ensure electrostatic interactions with several molecules including dyes molecules.

Influence of process parameters

The adsorption equilibrium is calculated by different processing parameters, such as solvent and adsorbent properties, pH, and the solution temperature. The first step in understanding the process is to refine the best operating parameters.

Effect of the solution pH

The pH of the solution is an essential parameter for monitoring the dye adsorption by influencing the adsorbent's

Table 1: Atomic and weight percentage fraction analysis of chemical elements obtained by EDAX.

Element	% by mass	% atomic	cal % by mass
C	49.71	64.6	56.12
N	18.77	23.32	18.71
Zn	27.04	7.2	21.84
O	4.48	4.88	0.00

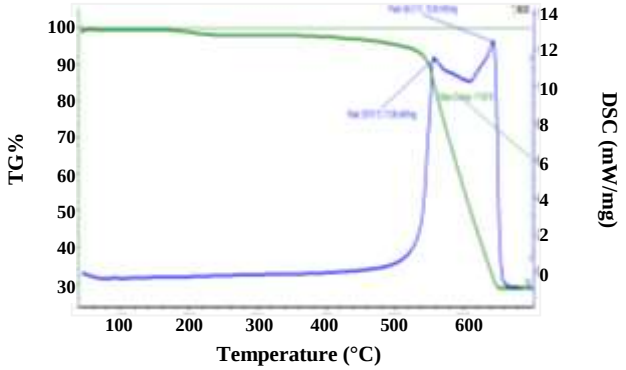

Fig. 4: TGA/DSC of prepared ZIF-11 crystals.

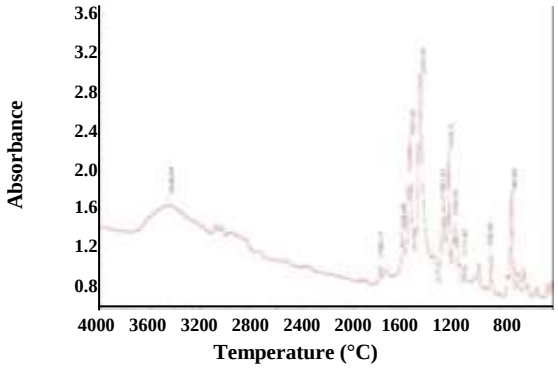

Fig. 5: FT-IR spectrum of prepared ZIF-11 crystals.

surface charge, the ionization degree of dyes, the dissociation of functional groups on the active sites of the adsorbent, and the structure of the dye molecule. Fig. 6 (A) shows the effect of initial pH on the percentage removal of MO onto ZIF-11 particles in a pH range of 2 to 12. Figure 6 (B) shows the point of zero charges (pH_{PZC}) of ZIF-11 particles, which was 8.1. There was a very small variation in the removal efficiency in both acidic and basic media. At a solution pH > 3.46, which corresponds to the MO pKa, the formed MO anions, due to the sulphonate groups ($SO3^-$) occurrence, might be attracted to the positively charged Zn atoms of the ZIF. The removal efficiency was recorded at its highest level (82%). In acidic media (pH < 3.46), the MO molecules presented the cationic form due to positively charged azo bonds (-N = N-) and banding of H^+ with $–SO_3^–$ to form–SO_3H. Similarly, the ZIFs particles, which have a dual Lewis acidic (Zn atom) and basic sites (-NH groups of the imidazolate linkers) [40, 41] might attract the H^+ protons to become mostly positively charged. This statement was supported by the increased value of the final solution pH (pH_f = 6 for pH_i at 4) indicating that the solution had diminished in H^+, a part of which reacted with MO, another with ZIF-11, and the remaining in the solution. Most likely, a competition resulted between different charged elements involving attraction and repulsion forces: the NH_3 groups of the ZIF-11 particles preferentially adsorbed the H^+ protons, which, like the Zn atoms of the ZIFs, might well attract SO_3 groups of MO molecules. However, the azo bonds (-N = N-) of the MO molecules would have been repulsed. Indeed, the challenge that is not easy to overcome did not increase the MO removal efficiency observed with other adsorbents [42].

Effect of the contact time

The influence of the contact time of adsorption MO on the ZIF-11 surface was studied by changing the contact time ranging from 5min to 60min at 22 ±2 °C, pH = 8.02, 20 mg of ZIF-11 dosage, and 20 mg/L of MO initial concentration. As shown in Fig. 7, rapid adsorption of MO occurred during the first 30 min after which the rate was reduced until the equilibrium was reached at 40 min, the adsorption capacity attained 27.64 mg/g, and the percentage removal of MO attained 82.91%. This result can be interpreted by the fact that all vacant sites on the adsorbent surface were eligible for rapid attachment of dye molecules during the initial adsorption time. As the adsorption process progressed, the number of empty sites reduced and there was repulsion between adsorbate molecules attached to the adsorbent and those in the bulk phase. The adsorption equilibrium process was reached

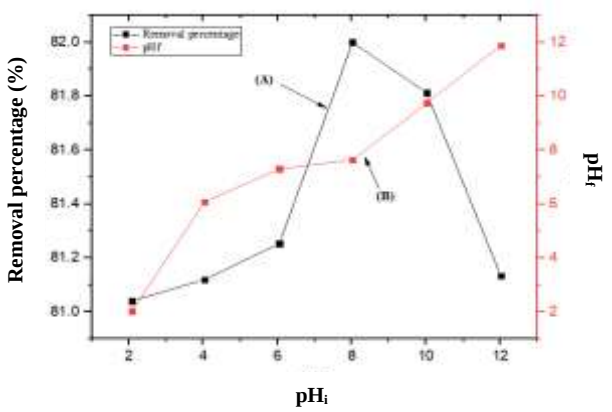

Fig. 6: Effect of pH on the removal percentage of MO-by ZIF-11 (A) (MO: 20 mg/L; adsorbent dosage: 400mg/L; temperature: 298 K; stirring speed: 400 rpm; contact time: 60 min) and determination of zero point charge of ZIF-11(B).

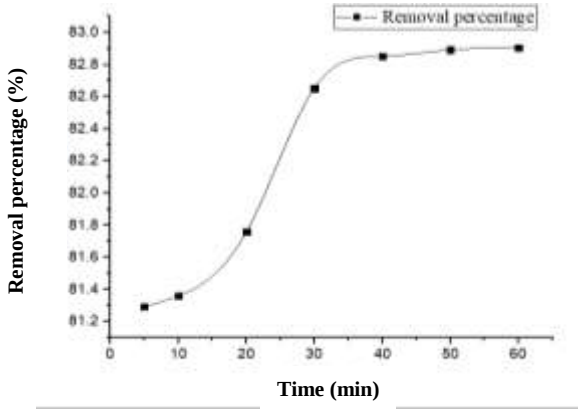

Fig. 7: Effect of contact time on the removal percentage of MO by ZIF-11, pH: 8.02; C_0: 20 mg/L; T: 22±2 °C.

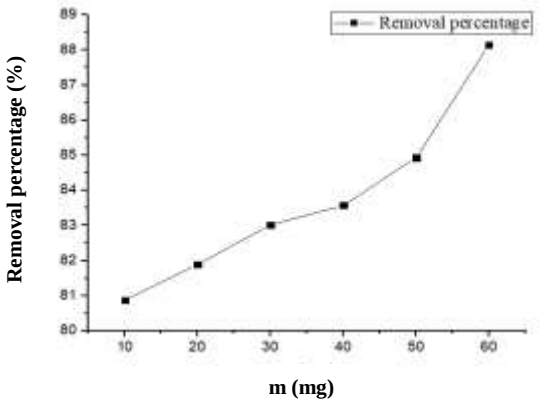

Fig. 8: Effect of ZIF-11 dosage on the removal percentage of MO, pH: 8.02; t: 40 min; C_0: 20 mg/L; T: 22±2 °C.

quickly. At this point, the rates of adsorption and desorption were equal and no apparent increase in the rate of removal could be seen. Similar trends were obtained for the adsorption of cationic methylene blue or anionic MO [33, 43].

Effect of the adsorbent dosage

The effect of adsorbent dosage on the adsorption capacity and the percentage removal of MO at an initial MO concentration of 20 mg/L was investigated and the results are shown in Fig. 8. It was found that the evolution of the percentage of MO removal (adsorption capacity) with the adsorbent dosage followed an increasing linear trend. A value of 88.15% was achieved, indicating the suitability of ZIF-11 as an adsorbent for MO. Thus, the increase in the available sorption surface and the capacity of the adsorption sites resulted in an increase in the % removal of OM. Similar conclusions were made for the adsorbent dosage for dye removal. It is noteworthy that for some adsorbents, high dosages caused agglomeration in the solution, which inhibited the evolution of the percentage of dye removal above an equilibrium [44, 45].

Influence of stirring speed

The influence of stirring speed over the range (200 – 900 rpm using a mechanical agitator and magnetic stirrer) on the adsorption capacity of MO from the solution onto ZIF-11 has been investigated and the results were described in Fig. 9. In batch adsorption processes, agitation speed plays an important role in influencing the external boundary film and the distribution of the solute in the solution phase. It was found that for a variation of the stirring speed from 200 rpm to 600 rpm the percentage of MO removal increased slightly from 86.8% to 88%. The MO molecules diffused efficiently onto the surface of ZIF-11 due to their solubility in water. However, the increase in removal percentage was stopped by an increased tendency for desorption of the dye molecules, which may occur for strong agitation [46].

Influence of initial MO concentration

The influence of the initial MO concentration on the removal percentage was evaluated for concentrations ranging from 20mg/L to 900 mg/L for a contact time of 40 minutes, a pH of 8.02, and a stirring speed of 600 rpm. The results showed that with increasing initial

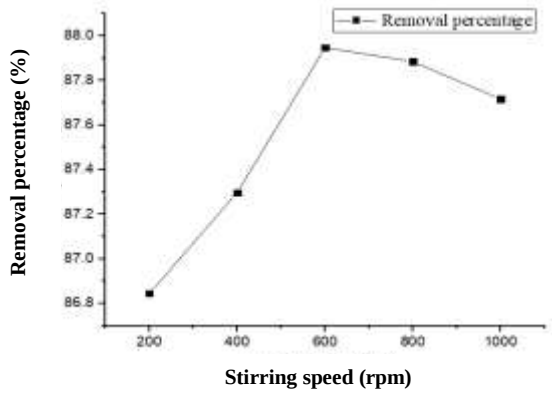

Fig. 9: Effect of stirring speed on the removal percentage of MO by ZIF-11, pH: 8.02; t: 40 min; C0: 20 mg/L; T: 22±2 °C.

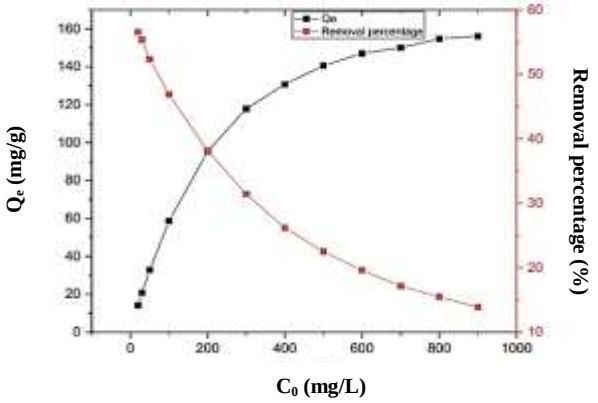

Fig. 10: Effect of initial concentration on the adsorption of MO onto ZIF-11 (pH ~ 8.02; stirring speed: 600 rpm; adsorbent dosage: 30mg; temperature: 298 K; contact time: 40 min).

concentration of MO its removal percentage decreased (Fig.10). Indeed, the low dosage of ZIF-11 (30mg) was not sufficient to adsorb all the MO molecules which became abundant as the initial concentrations were increased. Similar results have been observed previously for different types of adsorbents and adsorbates [47, 48]. The lack of active sites required for dye adsorption was also mentioned due to the excess of adsorbate molecules [50]. In such cases, cost-effective removal is achieved with solutions of low initial concentration, or with high adsorbent dosage, which in practice is consistent with environmental requirements.

Effect of temperature and adsorption thermodynamics

The effect of the temperature on the adsorptive capacity at equilibrium Q_e and removal percentage $R(\%)_e$ of MO was investigated and the results are summarized in Fig.11A. The MO removal percentage by ZIF-11 increased from 84.68% (362.91 mg/g of uptake) to 90.67% (388.58 mg/g of uptake) with increasing temperature from 23°C to 48°C and remained almost constant thereafter. The effect of thermal motion influenced the adsorption of MO by ZIF-11 because of the increased diffusion of MO molecules from the solution to the adsorbent surface and the low competitiveness of water molecules in adsorption on hydrophobic sites of ZIF-11. Thus, stable ion pair complexes could be formed between SO_3 groups of MO molecules and Zn atoms of the ZIF-11 particles. It has been reported that in the case of dye removal the adsorption is favorable at higher temperatures. Indeed, the increase in temperature increases, the mobility of the adsorbate molecules in the solution and the affinity of the adsorbate on the adsorbent is higher [15, 50]. This insight is so important for practical application, as most textile dye effluents are discharged at relatively high temperatures (50 – 60°C) [21].

The thermodynamic conduct of adsorption of MO onto ZIF-11 was evaluated through the thermodynamic parameters: Gibbs free energy change (ΔG°), enthalpy change (ΔH°), and entropy change (ΔS°), which were determined based on the classical Van't Hoff equation

$$\Delta G^\circ = -RTLnK_d = \Delta H^\circ - T\Delta S^\circ \quad (9)$$

Where K_d is the constant partition coefficient defined as [43] : $K_d = \frac{q_e}{c_e}$,

where R is the universal gas constant (8.314 J/mol K), T is the temperature in K.

Hence :

$$\ln K_d = \frac{\Delta S^\circ}{R} - \frac{\Delta H^\circ}{RT} \quad (10)$$

The slope and intercept of the linear plot (Fig. 11B) of lnK_d versus $1/T$ for MO adsorption at different temperatures onto ZIF-11 were used to evaluate the thermodynamic parameters (Table 2).

As seen in Table 2, the negative values of ΔG° indicated that the MO adsorption onto ZIF-11 was spontaneous and feasible, particularly for elevated temperatures. These findings confirmed the suggestion

Table 2: Thermodynamic study of the adsorption of MO dye onto ZIF-11 surface.

Temperature K	ΔG° (kJ/mol)	ΔH° (kJ/mol)	ΔS° (kJ/mol.K)
296	-3.381	16.80	0.068
314	-4.769		
321	-5.173		
324	-5.214		

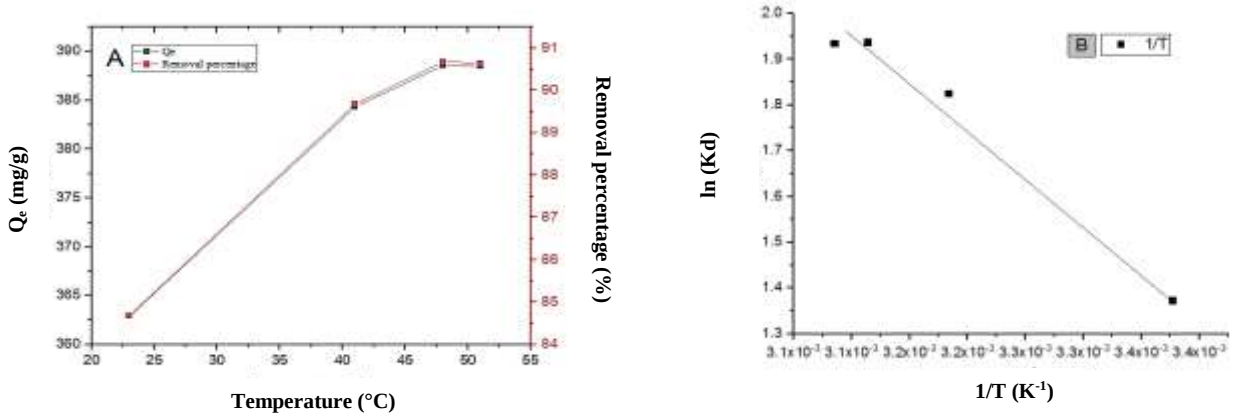

Fig. 11: Effect of temperature on the adsorption of MO onto ZIF-11 (A) and linear Plot of Ln(K_d) versus 1/T for the MO adsorption at different temperatures (B).

that the diffusion and affinity of OMmolecules on ZIF-11 particles increased with increasing temperature. The mobility of MO molecules in solution was also supported by the positive ΔS°, values, indicating increased randomness at the solid/solution interface and a good affinity of MO for ZIF-11. The positive value of ΔH^0 =16.80 kJ/mol indicated the endothermic nature of the MO adsorption onto ZIF-11. Indeed, heat supply was needed to desorb the previously adsorbed water molecules prior to the adsorption of the MO molecules onto the ZIF-11 particles. These results, in accordance with reports of dye adsorption studies on different adsorbents [50], are consistent with a physicochemical adsorption process.

Adsorption kinetics

The adsorption kinetics not only provide information on the rate of adsorption, which determines the time required to reach equilibrium in the adsorption process but also on the probable mechanisms involved. This is also important data for process development and adsorption system design [44]. In order to investigate the adsorption process of MO on ZIF-11, the Pseudo-First-Order (PFO) model (11), the Pseudo-Second-Order (PSO) model (12), and the intraparticle diffusion model (IP) were used (13).

$$\ln(q_e - q_t) = \ln q_e - k_1 t \quad (11)$$

$$\frac{t}{q_t} = \frac{1}{k_2 q_e^2} + \frac{t}{q_e} \quad (12)$$

$$q_t = k_p t^{0.5} + C \quad (13)$$

Where Q_t (mg/g) is the amount of the MO dye adsorbed at time t (min), k_1 is the rate constant of the equation (min^{-1}), k_2 (g/mg min) is the rate constant of the second-order equation. k_p (mg/ g $min^{0.5}$) is the intra-particle diffusion rate constant and C is the intercept for the linearized IP model.

The experimental data, which were recorded for a set of MO adsorption trials with an initial concentration of 20 mg/L, at contact times ranging from zero to 60 min, were fitted to these models. The linear plots related to the cited kinetic models are presented in Fig. 12 and the calculated values of the corresponding kinetic and statistic parameters, R^2, RMSE, SSE, χ^2, ARE, and MPSD are summarized in Table 3.

Table 3: Kinetic parameters obtained from various kinetic models for sorption of MO.

Statistical and kinetic Parameters	PFO model	PSO model	IP model
RMSE	0.091	0.207	0.614
SSE	0.008	0.043	0.377
χ^2	0.002	0.011	0.096
ARE	0.231	0.460	2.087
MSPD	0.003	0.007	0.022
R^2	0.955	1	(0.92÷ 0.94)
$(q_e)_{exp}$ (mg/g)	27.65	27.65	
q_{cal} (mg/g)	-	27.7	C = 26.81
k	0.0764	0.171	0.1166

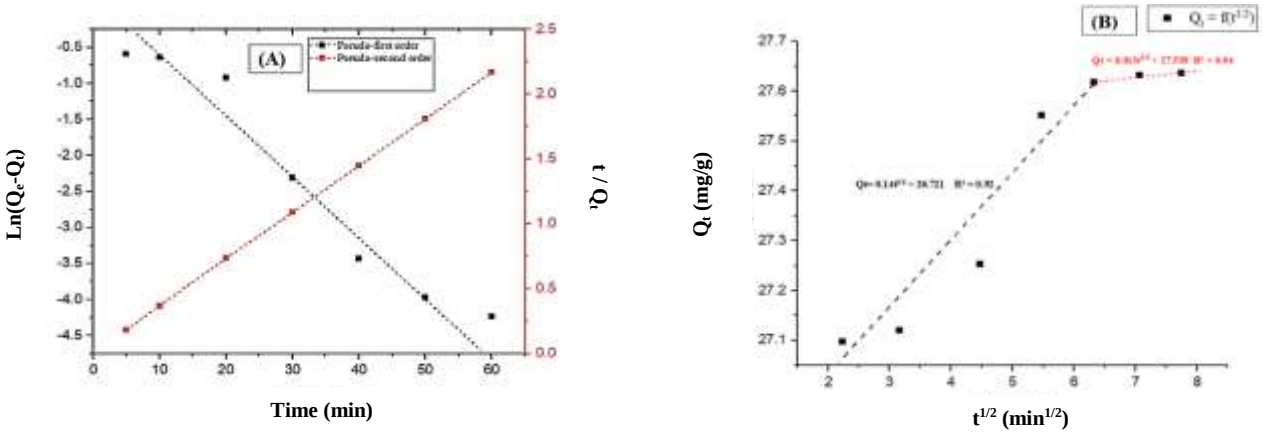

Fig. 12: Plots of fitted PFO and PSO linearized models (A) and IP diffusion linearized model (B) for MO adsorption onto ZIF-11.

The kinetic data analysis revealed that the PFO equation did not fit correctly over the full range of adsorption times, compared to the PSO equation, which matched perfectly. The adequacy of the PSO model was confirmed, on one hand, by the straight line obtained in the plot of $t/q_t = f(t)$ (fig.12) with $R^2 \approx 1$ and, on the other one, by the convergence of the values for q_e (Tab. 3). It has been reported that PSO model matches well with chemisorption processes occurring on homogeneous solid surfaces, whereas adsorption onto inhomogeneous solid surfaces is controlled by diffusion [51]. The PSO model was also well matched with the adsorption data of dyes, including MO, methylene blue, and methyl red onto ZIFs (ZIF-8, ZIF-67, and bimetallic Zn/Co ZIF). ZIF-67 proved to be the best adsorbent with q_e values not exceeding 11.72 mg/g for MO adsorption [4]. Thus, the analysis of kinetic data needs to be further enhanced, especially for controlled diffusion systems [52]. Thus, the IP diffusion model fitting showed a bi-linear plot with satisfactory statistical errors (Fig. 12 and Table 3). It can be assumed that the major part of the MO molecules adsorbs rapidly (during the first 30 min) on the external surface of ZIF-11 and then the other part of the molecules migrates progressively into the pores, where the intraparticle diffusion is controlled. This assumption is consistent with the mentioned heterogeneity of the synthesized ZIF-11 (section 3.1.2).

Adsorption isotherms

The Langmuir, Freundlich, Temkin, and Dubinin Radushkevich isotherm models (Dubinin- R) were used to study the adsorption of MO onto ZIF-11. The linearized equations of these models are given (13) – (16). The experimental adsorption equilibrium data were acquired by changing the initial concentrations of MO with fixed

Table 4: Isotherm model error analysis.

Model	RMSE	SSE	χ^2	ARE	MSPD	R^2
Langmuir	0.637	0.406	0.096	1.14	0.022	0.999
Freundlich	12.417	154.186	418.049	253.15	4.786	0.944
Temkin	6.635	44.03	1.127	16.51	1.917	0.992
Dubinin- R	15.873	251.945	76.566	31.17	2.752	0.884

dosage of adsorbent (800mg/L of MO solution), pH (~ 8.02), stirring speed (600 rpm), temperature (298 K); and contact time (40 min). The experimental data were fitted to the mentioned models, where the calculated error functions (MSPD, ARE, χ^2, SSE, RMSE) and the coefficient of determination (R^2) served to prove the most appropriate model. Table 4 summarizes the calculated values for these statistical criteria and Table 5 presents the calculated isotherms parameters.

$$\text{Langmuir isotherm} \quad \frac{1}{q_e} = \frac{1}{K_L q_m C_e} + \frac{1}{q_m} \tag{13}$$

$$\text{Freundlich isotherm} \quad \ln(q_e) = \ln K_F + \frac{1}{n}\ln C_e \tag{14}$$

$$\text{Temkin isotherm} \quad q_e = \frac{RT}{n}\ln K_T + \frac{RT}{n}\ln C_e \tag{15}$$

$$\text{Dubinin Radushkevich isotherm} \quad \ln(q_e) = \ln q_s - K_{ad}\varepsilon^2 \tag{16}$$

Where K_L (L/mg), K_F, K_T (L/mg), and K_{ad} (mg/kJ) are respectively the Langmuir, Freundlich, Temkin, and Dubinin Radushkevich equilibrium constants, q_m represents the maximum adsorption capacity of the adsorbent (mg/g), n^{-1} is the adsorption intensity and ε is the Polanyi potential described as:

$$\varepsilon = RT\ln\left(1+\frac{1}{C_e}\right) \tag{17}$$

R is the gas constant 8.314 10^{-3} kJ/mol K, T is the temperature, K.

The separation factor designed by R_L and given by equation (A18) indicates the adsorption nature to be either [53]

- Unfavorable if $R_L > 1$
- Linear if $R_L = 1$
- Irreversible if $R_L = 0$
- Favorable if $0 < R_L < 1$

$$R_L = \frac{1}{K_L q_m + C_0} \tag{18}$$

The mean free energy of adsorption per molecule of adsorbate required to transfer one mole of MO dye from the infinity in the solution to the surface of ZIF-11 can be calculated as [54] :

$$E = \frac{1}{\sqrt{2K_{ad}}} \tag{19}$$

According to the significant R^2 and standard error values (Table 4), compared to the Freundlich and Dubinin Radushkevich isotherms the Langmuir and the Temkin isotherms achieved the best fit between experimental and calculated data. Particularly, the low values for the Langmuir isotherm parameters ($K_L = 0.009\ L/mg$, $q_m = 178.57\ mg/g$ and $R_L = 0.019$) indicated a favorable MO adsorption onto ZIF-11. The same considerations can be slightly applicable to the Temkin isotherm involving a uniform distribution of the binding energy up to the maximum value. Therefore, it can be assumed that MO molecules were uniformly adsorbed on the active sites of ZIF-11 particles.

Comparison with Other ZIFs for MO sorption.

In order to show the advantage of ZIF-11 for the adsorption of MO from an aqueous solution, the results obtained in this study were compared with other investigations. Table 6 shows the maximum adsorption capacity of some considered adsorbents. The magnetic core-shell composite Fe3O4-PSS@ZIF-67 was found to be a powerful adsorbent of MO [49]. The microfluidic-synthesized chitosan microspheres with a capacity of 207 mg/g are also notable adsorbents [49]. However, considering the easy synthesis and higher adsorption performance of ZIF-11, it would be a promising adsorbent for the efficient removal of Mo from aqueous solutions.

Table 5: Adsorption isotherm parameters for the uptake of MO on ZIF-11.

Langmuir		Freundlich		Dubinin Radushkevich		Temkin	
q_m (mg/g)	178.57	K_f	10.090	q_s (mg/g)	195.547	K_t (L/mg)	0.104
K_L(L/mg)	0.009	n	2.307	K_{ad} (mg/kJ)	427.460	B (J/mol)	66.930
R_L	0.019			E (kJ)	0.034		

Table 6: Comparison of methyl orange adsorption capacity of ZIF-11 with some other adsorbents.

Adsorbent	Adsorption capacity (mg/g), References
ZIF-08	7.35 [55]
ZIF-67	4.69 [55]
Magnetic core-shell composite Fe_3O_4-PSS@ZIF-67	738 [55]
Microfluidic-synthesized chitosan microspheres	207 [56]
Amino-functionalized Zr-based MOFs	148.4 [57]
Nickel oxide nanoflakes NiONPs	165.83 [58] ; 188.68 [59]
Copper oxide nanoflakes CuO NPs	158.73 [58] ; 121.95 [59]
Hollow molybdenum disulfide (h-MoS_2) microspheres	41.52 [60]
ZIF-11	178.57 This study

CONCLUSIONS

In this work, Zeolitic Imidazolate Frameworks -11 (ZIF-11) were successfully synthesized via a room temperature process. The XRD, SEM/EDAX, ATG/DSC, and FT-IR characterizations revealed high crystallinity, morphology, and thermal stability of this molecular porous material, which motivated its use for MO removal from an aqueous solution. The effects of adsorption parameters were studied and the maximum removal percent was achieved at pH=8, stirring speed of 600 rpm, for a contact time of 40min, and a dosage of 40mg ZIF-11 for 50ml of MO solution.

The adsorption process was spontaneous and endothermic, and its kinetics can be profitably fitted to the pseudo-second-order kinetic model. Furthermore, the equilibrium data were best illustrated by the Langmuir and Temkin isotherm models indicating that MO molecules were uniformly adsorbed on the active sites of ZIF-11 particles. The maximum adsorption capacity of MO onto ZIF-11 particles (178.57 mg/g) was considered with respect to the values obtained for other laboratory experiments with adsorbents. Thus, the synthesized ZIF-11 would have potential adsorptive properties for MO dyes.

Declaration of competing interest

We declare that we have no financial or personal relationships with other people or organizations that can inappropriately influence our work; there is no professional or other personal interest of any nature or kind in any product, service, and/or company that could be construed as influencing the position presented in, or the review of, the manuscript entitled.

Acknowledgments

The authors express their appreciation to the Algerian Directorate General for Scientific Research and Technological Development (DGRSDT) for the financial support of this work.

Received : Jul. 16, 2021 ; Accepted : Sep. 19, 2021

REFERENCES

[1] Park K.S., Ni Z., Cote A.P., Choi J.Y., Huang R., Uribe-Romo F.J., Chae H.K., O'keeffe M., Yaghi O.M, Exceptional Chemical and Thermal Stability of Zeolitic Imidazolate Frameworks, *PNAC*., **103(27)**: 10186–10191 (2006).

[2] Chen B., Yang Z., Zhu Y., Xia Y., Zeolitic Imidazolate Framework Materials: Recent Progress in Synthesis and Applications *J. Mater. Chem. A*, **2**: 16811-16831 (2014).

[3] Bhattacharjee S., Jang M-S., Kwon H-J., Ahn W-S., Zeolitic Imidazolate Frameworks: Synthesis, Functionalization, and Catalytic/Adsorption Applications. *Catal. Surv. Jpn.*, **18**: 101–127 (2014).

[4] Noor T., Raffi U., Iqbal N., Yaqoob L., Zaman N., Kinetic Evaluation and Comparative Study of Cationic and Anionic Dyes Adsorption on Zeolitic Imidazolate Frameworks Based Metal Organic Frameworks, *Mater. Res. Express*, **6(12)**: 1-26 (2019).

[5] Miensah E.D., Muhammad Khan M., Chen J.Y., Mei Zhang X, Wang P., Zhang Z.X., Jiao Y., Liu Y., Yang Y., Zeolitic Imidazolate Frameworks and their Derived Materials for Sequestration of Radionuclides in the Environment: A Review, *Crit. Rev. Environ. Sci. Technol*., **50(18)**: 1874-1934 (2020).

[6] Sutrisna P. D., Savitri E., Himma N. F., Prasetya N., Wenten I.G., Current Perspectives and Mini Review on Zeolitic Imidazolate Framework-8 (ZIF-8) Membranes on Organic Substrates, *IOP Conf, Ser.: Mater. Sci. Eng*., **703**: 012045(2019).

[7] Zhang J., Tan Y., Song WJ., Zeolitic Imidazolate Frameworks for Use In Electrochemical and Optical Chemical Sensing and Biosensing: A Review, *Microchim. Acta*, **187**: 234 (2020).

[8] Hajializadeh A., Ansari M., Foroughi M., Jahani S., Kazemipour M., Zeolite Imidazolate Framework Nanocrystals Electrodeposited on Stainless Steel Fiber for Determination of Polycyclic Aromatic Hydrocarbons, *Iran. J. Chem. Chem. Eng. (IJCCE)*, **41(2)**: 368-372 (2022).

[9] Pimentel B.R., Jue M.L., Zhou E.K., Ross J. Verploegh, Johannes Leisen, David S. Sholl, and Ryan P. Lively, Sorption and Transport of Vapors in ZIF-11: Adsorption, Diff usion, and Linker Flexibility, *J. of Phys. Chem. C*, **123(20)**:12862-12870 (2019).

[10] Gong Y., Tang Y., Mao Z., Wu X., Liu Q., Hu S., Wang X., Metal-Organic Framework Derived Nanoporous Carbons with Highly Selective Adsorption and Separation of Xenon, *J. of Mater. Chem. A*, **6(28)**: 13696–13704 (2018).

[11] E.M. Forman, A. Baniani, L. Fan, K.J. Ziegler, E. Zhou, F. Zhang, R.P. Lively, S. Vasenkov, Ethylene Diffusion in Crystals of Zeolitic Imidazole Framework-11 Embedded in Polymers to Form Mixed-Matrix Membranes, *Microporous Mesoporous Mater*., **274**: 163-170 (2018).

[12] Chandra R., Nath M., Facile Synthesis of Metal–Organic Framework (ZIF- 11) and Ag NPs Encapsulated- ZIF- 11 Composite as an Effective Heterogeneous Catalyst for Photodegradation of Methylene Blue, *Appl. Organomet. Chem*., **34(11)**: e5951 (2020).

[13] Katheresan V., Kansedo J., Lau S.Y., Efficiency of Various Recent Wastewater Dye Removal Methods: A Review, *J. of Environ. Chem. Eng*., **6(4)**: 4676-4697 (2018).

[14] Khan T.A., Rahman R., Khan E.A., Adsorption of Malachite Green and Methyl Orange Onto Waste Tyre Activated Carbon Using Batch and Fixed-Bed Techniques: Isotherm and Kinetics Modeling, *Model. Earth Syst. Environ*. **3**: 38 (2017).

[15] Khan E.A., Shahjahan, Khan T.A., Synthesis of Magnetic Iron - Manganese Oxide Coated Graphene Oxide and its Application for Adsorptive Removal of Basic Dyes from Aqueous Solution: Isotherm, Kinetics, and Thermodynamic Studies, *Environ. Prog. & Sustainable Energy*, **38(S1)**: S214 - S229 (2018).

[16] Tajizadegan H., Torabi O., Heidary A., Golabgir M.H., Jamshidi A., Study of Methyl Orange Adsorption Properties on ZnO–Al_2O_3 Nanocomposite Adsorbent Particles, *Desalination and Water Treatment*, **57(26)**: 12324-12334 (2016).

[17] Du X-D., Wang C-C., Liu J-G., Zhao X-D., Zhong J, Li Y-X., Li J., Wang P., Extensive and Selective Adsorption of ZIF-67 Towards Organic Dyes: Performance and Mechanism, *J. Colloid Interface Sci*., **506**: 437–41 (2017).

[18] Malviya A., Jaspal D., Sharma P., Dubey A., Isothermal Mathematical Modeling for Decolorizing Water - A Comparative Approach., *Sustain. Environ. Res*., **25**: 53–58 (2015).

[19] Sabnis R.W., Handbook of Acid-Base Indicators, *Taylor & Francis Group, LLC*., 228–229 (2008).

[20] Feng J., Cerniglia C.E., Chen H., Toxicological Significance of Azo Dye Metabolism by Human Intestinal Microbiota, *Frontiers in Bioscience (Elite edition)*, **4**: 568–586 (2012).

[21] Z. Aksu, Application of Biosorption for the Removal of Organic Pollutants: A Review, *Process Biochem.* **40**: 997–1026 (2005).

[22] León G., García F., Miguel B., Bayo J., Equilibrium, Kinetic and Thermodynamic Studies of Methyl Orange Removal by Adsorption onto Granular Activated Carbon, *Desalination and Water Treat*., **57(36)**: 17104-17117 (2016).

[23] Pal J., Deb M.K., Deshmukh D.K., Verma D., Removal of Methyl Orange by Activated Carbon Modified by Silver Nanoparticles, *Appl. Water Sci.*, **3**: 367–374 (2013).

[24] Mokhtari P., Ghaedi M., Dashtian K., Rahimi M. R., Purkait M. K., Removal of Methyl Orange by Copper Sulfide Nanoparticles Loaded Activated Carbon: Kinetic And Isotherm Investigation, *J. of Mol. Liq*., **219**: 299-305 (2016).

[25] Wu Y., Su M., Chen J., Xu Z., Tang J., Chang X., Chen, Superior Adsorption of Methyl Orange by h-MoS2 microspheres: Isotherm, Kinetics, and Thermodynamic Studies, *Dye. and Pigm.*, **170**: 107591 (2019).

[26] Yang Q., Ren S., Zhao Q., Lu R., Hang C., Chen Z., Zheng H., Selective Separation of Methyl Orange From Water Using Magnetic ZIF-67 Composites, *Chem. Eng. J*., **333**:49–57 (2018).

[27] Li Y., Zhou K., He M., Yao J., Synthesis of ZIF-8 and ZIF-67 Using Mixed-Base and their Dye Adsorption, *Microporous and Mesoporous Mater*., **234**: 287-292 (2016).

[28] Hu H., Liu S., Chen C., Wang J., Zou Y., Lin L., Yao S., Two Novel Zeolitic Imidazolate Frameworks (ZIFs) as Sorbents for Solid-Phase Extraction (SPE) of Polycyclic Aromatic Hydrocarbons (PAHs) in Environmental Water Samples, *The Analyst*, **139(22)**: 5818–5826 (2014).

[29] Forman E.M., Pimentel B.R., Ziegler K.J., Lively R.P., Vasenkov S., Microscopic Diffusion of Pure and Mixed Methane and Carbon Dioxide in ZIF-11 by High Field Diffusion NMR, *Microporous and Mesoporous Materials*, **248**: 158–163 (2017).

[30] He M., Yao J., Liu Q., Zhong Z., Wang H., Toluene-Assisted Synthesis of RHO-Type Zeolitic Imidazolate Frameworks: Synthesis And Formation Mechanism of ZIF-11 and ZIF-12, *Dalton Trans*., **42**: 16608-16613 (2013).

[31] Nimibofa Ayawei, Augustus Newton Ebelegi, Donbebe Wankasi, Modelling and Interpretation of Adsorption Isotherms, *J. of Chem.,* **2017**, Article ID 3039817, **11** (2017).

[32] Paluri P., Ahmad K.A., Durbha K.S., Importance of Estimation of Optimum Isotherm Model Parameters for Adsorption of Methylene Blue onto Biomass Derived Activated Carbons: Comparison Between Linear and Non-Linear Methods, *Biomass Conv. Bioref.*, 1-18 (2020).

[33] Feng Y., Li Y., Xu M., Liu S., Yao J., Fast Adsorption of Methyl Blue on Zeolitic Imidazolate Framework-8 and Its Adsorption Mechanism, *RSC Adv.*, **6**: 109608-109612 (2016).

[34] He M., Yao J., Liu Q., Zhong Z., Wang H., Toluene-Assisted Synthesis of RHO-Type Zeolitic Imidazolate Frameworks: Synthesis and Formation Mechanism of ZIF-11 and ZIF-12, *Dalton Trans*, **42**:16608-16613 (2013).

[35] Sanchez-Lainez J., Zornoza B., Mayoral A., Berenguer-Murcia Á., CazorlaAmorós D., Tellez C., Coronas J., Beyond the H_2/CO_2 Upper Bound: One-Step Crystallization and Separation of Nano-Sized ZIF-11 by Centrifugation and its Application in Mixed Matrix Membranes, *J. Mater. Chem. A 7*., 6549–6556 (2015).

[36] Kim M.R., Kim T., Rye H.S., Lee W., Kim H. G., Kim M.I., Lim C.S., Zeolitic Imidazolate Framework Promoters in One-Pot Epoxy–Amine Reaction, *J. Mater Sci*., **55**:2068–2076 (2020).

[37] Safak Boroglu M., Structural Characterization and Gas Permeation Properties of Polyetherimide (PEI) Zeolithic Imidazolate (ZIF-11) Mixed Matrix Membranes, *J. of the Turkish Chem. Soc., Section A: Chem*., **3(2)**:183-206 (2016).

[38] He M., Yao J., Li L., Wang K., Chen F., Synthesis of Zeolitic Imidazolate Framework-7 in a Water/Ethanol Mixture and its Ethanol-Induced Reversible Phase Transition, *Chem. Plus. Chem*., **78**: 1222–1225 (2013).

[39] Cheng J., Ma D., Li Sh., Qu W., Wang D., Preparation of Zeolitic Imidazolate Frameworks and Their Application as Flame Retardant and Smoke Suppression Agent for Rigid Polyurethane Foams, *Polymers*, **12**: 347 (2020).

[40] Yumru A.B., Boroglu M.S., Boz I., ZIF-11/Matrimid® Mixed Matrix Membranes for Efficient CO_2, CH_4 and H_2 Separations, *Greenhouse Gas Sci. Technol*., **8**: 529-541(2018).

[41] Lin Y.F., Huang K.-W., Ko B.-T., Andrew Lin K.-Y., Bifunctional ZIF-78 Heterogeneous Catalyst with Dual Lewis Acidic and Basic Sites for Carbon Dioxide Fixation Via Cyclic Carbonate Synthesis, *J. of CO_2 Utilization*, **22**: 178-183 (2017).

[42] Xie X., Huang X., Lin W., Chen Y., Lang X., Wang Y., Gao L., Zhu H., and Chen J., Selective Adsorption of Cationic Dyes for Stable Metal–Organic Framework ZJU-48, *ACS Omega*, **5(23)**: 13595-13600 (2020).

[43] Shah S.S., Sharma T., Dar B.A., Bamezai R.K., Adsorptive Removal of Methyl Orange Dye From Aqueous Solution Using Populous Leaves: Insights from Kinetics, Thermodynamics and Computational Studies, *Environ. Chem. and Ecotoxicol*., **3**: 172-181 (2021).

[44] Zhao P., Zhang R., Wang J., Adsorption of Methyl Orange from Aqueous Solution Using Chitosan/ Diatomite Composite, *Water Sci. Technol.*,**75(7)**: 1633–1642 (2017).

[45] Haitham K., Razak S., Nawi M.A., Kinetics and Isotherm Studies of Methyl Orange Adsorption by a Highly Recyclable Immobilized Polyaniline on a Glass Plate, *Arabian J. of Chem*., **12(7)**: 1595-1606 (2019).

[46] Adeyemo A.A., Adeoye I.O., Bello O.S., Adsorption of Dyes Using Different Types of Clay: A Review, *Appl. Water Sci.*, **7**: 543–568 (2017).

[47] Ali Fil B., Ozmetin C., Adsorption of Cationic Dye from Aqueous Solution by Clay as an Adsorbent: Thermodynamic and Kinetic Studies, *J. Chem. Soc. Pak.*, **34**(4):897 (2012).

[48] Ma J., Jia Y., Jing Y., Yao Y., Sun J., Kinetics and Thermodynamics of Methylene Blue Adsorption by Cobalt-Hectorite Composite, *Dyes and Pigm*., **93**: 1441-1446 (2012).

[49] Pathania D., Sharma S., Singh P., Removal of Methylene Blue by Adsorption onto Activated Carbon Developed from Ficus Carica Bast, *Arabian J. of Chem*., **10(1)**: S1445–S1451 (2013).

[50] Saha P., Chowdhury Sh., Insight into Adsorption Thermodynamics. in: Mizutani Tadashi (Eds.), *Thermodynamics Chap*., **16**: 349-364 (2011).

[51] Ho Y., McKay G., Pseudo-Second Order Model for Sorption Processes, *Process Biochem*., **34**: 451–465 (1999).

[52] Simonin J.P., On the comparison of Pseudo-First Order and Pseudo-Second Order Rate Laws in the Modeling of Adsorption Kinetics, *Chem. Eng. J*., **300**: 254-263 (2016).

[53] Hall K. R., Eagleton L. C., Acrivos A., Vermeulen T., Pore and Solid Diffusion Kinetics in Fixed Bed Adsorption under Constant Pattern Conditions, *Ind. & Eng. Chem. Fundam*., **5**(2): 212-223 (1966).

[54] Hobson J.P., Physical Adsorption Isotherms Extending from Ultra-High Vacuum to Vapor Pressure, *J. Phys. Chem*. **73**: 2720– 2727 (1969).

[55] Yang Q., Ren S., Zhao Q., Lu R., Hang C., Chen Z., Zheng H., Selective Separation of Methyl Orange from Water Using Magnetic ZIF-67 Composites, *Chem. Eng. J*., **333**:49–57 (2018).

[56] Shi-Wen Lv, Jing-Min L., Hui Ma, Zhi-Hao W., Chun-Yang Li, Ning Z., Shuo W., Simultaneous Adsorption of Methyl Orange and Methylene Blue from Aqueous Solution Using Amino Functionalized Zr-based MOFs, *Microporous and Mesoporous Mater.*, **282**: 179-187 (2019).

[57] Yogesh Kumar K., Archana S., Vinuth Raj T.N., Prasana B.P., Raghu M.S., Muralidhara H.B., Superb Adsorption Capacity of Hydrothermally Synthesized Copper Oxide and Nickel Oxide Nanoflakes Towards Anionic and Cationic Dyes. *J. of Sci.: Adv. Mate. and Devices*. **2**: 183-191 (2017).

[58] Zhai L., Bai Z., Zhu Y., Wang B., Luo W., Fabrication of Chitosan Microspheres for Efficient Adsorption of Methyl Orange, *Chinese J. of Chem. Eng*., **26(3)**: 657-666 (2018).

[59] Darwish A.A.A., Rashad M., Hatem A. AL-Aoh., Methyl Orange Adsorption Comparison on Nanoparticles: Isotherm, Kinetics, and Thermodynamic Studies. *Dye and Pigm*., **160**: 563–571 (2019).

[60] WuY., Su M., Chen J., Xu Z., Tang J., Chang X., Chen D., Superior Adsorption of Methyl Orange by h-MoS_2 Microspheres: Isotherm, Kinetics, and Thermodynamic Studies, *Dye and Pigm*., **170**: 107591 (2019).